Available online at www.sciencedirect.com
ScienceDirect
Cement and Concrete Research 37 (2007) 131 – 138
Cement and Concrete Research

Multiphasic finite element modeling of concrete hydration

L. Buffo-Lacarrière [a,b], A. Sellier [b,*], G. Escadeillas [b], A. Turatsinze [b]

[a] VINCI Construction Grands Projets, 5 cours Ferdinand de Lesseps, F-92851 Rueil-Malmaison Cedex, France
[b] Laboratoire Matériaux et Durabilité des Constructions, INSA–UPS, 135 avenue de Rangueil, F-31077 Toulouse Cedex 4, France

Received 28 June 2006; accepted 8 November 2006

Abstract

This paper presents a model predicting the development of hydration and its consequences on temperature and water content. As it considers the effects of climatic conditions, the proposed model is a promising tool to evaluate the temperature, hydric and hydration fields of structures in situ.

The hydration model predicts the hydration evolution of several main species (not only clinker but also mineral additions like fly ash or silica fume for instance). For each component, the modeling considers hydration development and chemical interaction between reactions. It also takes into account temperature and water content effects on reaction kinetics through thermal and hydric activation. Hydration development in turn modifies the thermal and hydric states of material. The result is a numerical model coupling hydration, and the thermal and hydric states of cement-based material.

The model was tested on a 27 m^3 concrete block in situ equipped with temperature sensors situated in the core and close to the face exposed to solar radiation.

Keywords: Hydration kinetics; Modeling; Cement; Mineral additions; Temperature; Finite element analysis

1. Introduction

This paper assesses the hydration of cement or composed binders in massive structures. The work presented here is part of a larger research program the goal of which is to prevent concrete cracking at early age. While hardening, a structure is exposed to a risk of cracking which could have several origins: temperature gradient, autogenous or drying shrinkage gradient, restrained strains, etc., most of which are linked to binder hydration development. It is thus necessary to forecast the hydration evolution of cements, which are increasingly being used in civil engineering. As these cements are composed of various products (clinker, fly ash, silica fume, etc.) having different heat activation and kinetics, it is necessary to take into account their proportions for hydration modeling. This is the reason why a multiphasic model is proposed in this work.

Several multicomponent hydration models based on microstructure modeling have been proposed previously (CEMHYD3D [1], DUCOM [2] or even HYMOSTRUC [3]). These models are usually used to describe the microstructure evolution during hardening with great realism but they require long computing time, which is not really appropriate for applications in structural finite element modeling with a large number of nodes. As our study focuses on temperature and hydration development in massive structures in situ, we think that a good compromise between precision and workability can be reached using a multiphasic macroscopic model with a basic hydration law for clinker and additional laws for the hydration of each mineral addition.

The literature reports models using separate global laws for the reactions of clinker and additions. De Schutter [4,5], for instance, proposes a model of hydration for cements composed of clinker and slag while Kishi [6] models the hydration of cement mixed with fly ash. These models reproduce the combined hydrations of these species well but do not explicitly take account of the effect of water content on hydration.

This effect is nevertheless very important and not only modifies the final degree of hydration [7,8] but also the hydration kinetics [9]. It cannot be neglected for a realistic prevision of concrete hydration in a structure. Several authors

* Corresponding author. Tel.: +33 561 55 60 06.
E-mail address: alain.sellier@insa-toulouse.fr (A. Sellier).

0008-8846/$ - see front matter © 2006 Elsevier Ltd. All rights reserved.
doi:10.1016/j.cemconres.2006.11.010

report this essential effect of water content on hydration and propose models coupling hydration development and water content variation in structures [9,10].

Waller's works [11] combine the effects of water and mineral addition content. He proposes different hydration laws for clinker on the one hand and for pozzolanic additions (fly ash and silica fume) on the other. In each kinetic law, he adds an attenuation parameter depending on the water-to-binder ratio, which limits the degree of hydration to a final value depending on the initial water content. However this asymptotic approach cannot take account of, for instance, desiccation or rehydration effects during hydration.

These considerations lead us to propose a multiphasic approach for hydration modeling. This approach allows us to combine, at any instant, the effects of temperature and water content on the hydration of several solid phases (clinker and mineral additions for instance) including drying or rehydration periods.

The first part of this paper presents this multiphasic model and, in the second part, the model is applied to a real instrumented structure in order to be validated. This application also points out the importance of the thermal boundary conditions for temperature variations in the concrete block. It especially shows the influence of daily temperature variations and solar radiation effects, which are rarely taken into account in models. A parametric study also shows the positive effect of fly ash on the temperature gradient in the massive structure.

2. Multiphasic model presentation

The development of chemical reactions between clinker, pozzolanic or hydraulic additions (silica fume, fly ash, slag, etc.) and water is described using a scalar variable α_i, which refers to the hydration degree of anhydrous phase *i*. This variable is defined as the mass of anhydrous substance which has reacted per unit volume divided by the initial mass. The law for the variation of the degree of hydration is given by Eq. (1). The different components of the hydration kinetic law *F* will be presented in Section 2.1.

Water content is computed using the total water mass balance equation (Eq. (2)).

Temperature is determined by resolving the heat balance expressed by Eq. (3).

$$\begin{cases} \dot{\vec{\alpha}} = \vec{\mathsf{F}}(\vec{\alpha}, W, T) & (1) \\ \dot{W} = div(-D_{\mathrm{w}} \cdot \overrightarrow{\mathrm{grad}} W) + \vec{Q}_{\mathrm{th}}^{W} \cdot \dot{\vec{\alpha}} & (2) \\ \rho c \cdot \dot{T} = div(-\lambda \cdot \overrightarrow{\mathrm{grad}} T) + \vec{Q}_{\mathrm{th}}^{T} \cdot \dot{\vec{\alpha}} & (3) \\ +\text{boundary and initial conditions} \end{cases}$$

Where:

$$-\begin{cases} {}^{t}\vec{\alpha} = (\alpha_1 \cdot\cdot \alpha_i \cdot\cdot \alpha_n) \\ {}^{t}\vec{\mathsf{F}} = (\mathsf{F}_1 \cdot\cdot \mathsf{F}_i \cdot\cdot \mathsf{F}_n) \\ {}^{t}\vec{Q}_{th} = (Q_{\mathrm{th}_1} \cdot\cdot Q_{\mathrm{th}_i} \cdot\cdot Q_{\mathrm{th}_n}) \end{cases} \text{ and } \begin{vmatrix} i = 1 \rightarrow \text{clinker} \\ i = 2 \cdot\cdot n \rightarrow \text{reactive mineral additions} \end{vmatrix}$$

- α_i is the degree of hydration
- W is the total water content of the concrete
- D_{w} is the water transfer coefficient
- $Q_{\mathrm{th}_i}^{W}$ is the water needed for total hydration of anhydrous phase "*i*"
- T is temperature
- λ is thermal conductivity
- ρ is density
- c is specific heat
- $Q_{\mathrm{th}_i}^{T}$ is the heat produced by complete hydration of anhydrous phase "*i*"

2.1. Hydration kinetic law

The hydration kinetics is the result of two antagonistic physical phenomena. On the one hand supersaturation of the interstitial solution accelerates hydrate precipitation and thus increases the global hydration kinetics. On the other hand, as hydration reactions are possible only if water and reactive ions are present, the hydration kinetics is decreased by the difficulty of contact between water and anhydrous grains surrounded by a hydrated layer.

In the first stages of hydration, as only a few solid hydrated phases have been produced, hydration is mainly driven by acceleration due to supersaturation, while, beyond a critical degree of hydration, a decrease of the kinetics due to hydrate formation will become preponderant.

It should be noted that the increase in kinetics due to supersaturation or to temperature is rather a chemical phenomenon. Therefore, it is necessary to use different parameters in function c_i (Eq. (4)) in order to reproduce the different response of each anhydrous phase to these increasing effects. In contrast, the function Π_i models the facility of contact between water and the anhydrous grains and uses some parameters which are common to all anhydrous phases. Indeed, this function models the decrease in the kinetics during hydration due to hydrate formation, which limits water microtransfer between the porosity (common to all anhydrous phases) and the residual anhydrous phase.

In addition to these chemo-physical considerations, reactions of dissolution and hydrate formation are activated by environmental conditions. Thermal activation is thus represented by the function $h_i(T)$ while precipitation activation due to supersaturation of the interstitial solution is modeled by c_i (Eq. (4)). A delaying parameter (g_i) is added in the case of secondary reactions such as pozzolanic ones. It depends on the amounts of some primary reaction products (like portlandite for pozzolanic reactions) and will thus be linked to the primary reaction kinetics.

$$\dot{\alpha}_i = A_i \cdot \Pi_i(\bar{r}_m) \cdot c_i(\alpha, W) \cdot h_i(T) \cdot g_i \quad (4)$$

With: A_i a fitting parameter linked to the acceleration of the reaction kinetics due to supersaturation.

This hydration kinetics equation is representative of all anhydrous phases during concrete hardening. It could be used for coupling the hydration of clinker with reactions of mineral additions (fly ash, silica fume, etc.). Specific characteristics of each type of anhydrous material are taken into account by parameters of independent functions.

For the materials studied (Portland cement CEM I and fly ash), we propose to use following expressions (Eqs. (5), (6), (10) and (11)).

2.1.1. Water accessibility to anhydrous phase

In Eq. (4), Π_i models the water accessibility to anhydrous phases. We assess it using Eq. (5).

$$\Pi_i = \exp(-B_i \cdot \overline{r}_{m_i}^{n_i}) \tag{5}$$

Where:

- B_i and n_i are calibration parameters
- $\overline{r}_{m_i}$ is a function of water content, porosity and solid phases in the paste (Eq. (6)).

This function Π_i varying between 0 and 1, depends on the variable $\overline{r}_{m_i}$ (defined in the interval $[0, +\infty[$) which increases to model the increasing difficulty of access of free water to an anhydrous grain.

For sufficient degrees of hydration, the function Π_i models a deceleration period when the hydrate layers surrounding the anhydrous grains progressively separate the reacting anhydrous phase from water. The variable $\overline{r}_{m_i}$ is thus increased by the development of hydrates (Eq. (6)).

Water accessibility to anhydrous grains is also decreased by the closing of pores (Eq. (6)). The hydration kinetics is consequently reduced and hydration reactions could even be stopped if there is not enough space available for hydrate development (closed porosity) [7,8]. Lastly, the distance between water and anhydrous grains is obviously increased by the diminution of the water or anhydrous content.

The dependence of the hydration kinetics on water modeled by this function of $\overline{r}_{m_i}$ simulates the hydration limitation observed experimentally in the cases of both sealing material [11,12] and drying concrete.

Regarding these physical considerations, we chose the following expression (Eq. (6) for the variable $\overline{r}_{m_i}$.

$$\overline{r}_{m_i} = \frac{C_{\mathrm{p}_{hydr_i}}}{W_\mathrm{p} \cdot \Phi_\mathrm{p} \cdot C_{\mathrm{p}_{anh_i}}} \tag{6}$$

Where:

- W_p is the volumetric concentration of water in the paste porosity
- Φ_p is the porosity of paste
- C_{phydr_i} is the volumetric concentration of hydrate produced from grains of phase "i"
- $C_{\mathrm{p}anh_i}$ is anhydrous volumetric concentration in paste

In this equation, the numerator represents parameters decreasing the kinetics while the denominator contains parameters increasing it.

The volumetric concentrations of hydrates and the anhydrous phase are determined using Eqs. (7) and (8).

$$C_{\mathrm{p}_{hydr_i}} = R_i \cdot \alpha_i \cdot \frac{m_i}{V_{paste_{\mathrm{ini}}} \cdot \rho_i} \tag{7}$$

$$C_{\mathrm{p}_{anh_i}} = (1-\alpha_i) \cdot \frac{m_i}{V_{paste_{\mathrm{ini}}} \cdot \rho_i} \tag{8}$$

Where:

- $V_{paste_{\mathrm{ini}}}$ is the initial paste volumetric concentration in concrete
- R_i is volume ratio between hydrates and anhydrous phase for the species "i" (cement or fly ash)
- m_i is initial mass of anhydrous phase "i"
- ρ_i is anhydrous phase density

Paste porosity is determined by Eq. (9).

$$\Phi_\mathrm{p} = 1 - \sum_i (C_{\mathrm{p}_{hydr_i}} + C_{\mathrm{p}_{anh_i}}) \tag{9}$$

2.1.2. Thermal activation

In order to model temperature effects on the hydration kinetics (represented by h_i in Eq. (4)), we chose to apply the Arrhenius law (Eq. (10)), which is classically used to describe the influence of temperature on many chemical and physical processes [13].

$$h_i = \exp\left(-\frac{E_{\mathrm{a}_i}}{RT}\right) \tag{10}$$

Where:

- E_{a_i} is the activation energy of phase "i"
- R is the gas constant (8.314 J/mol K).

2.1.3. Chemical activation

As seen previously, in the first stage of hydration, chemical reactions are accelerated. Indeed supersaturation of the interstitial solution accelerates the precipitation of new hydrates [14].

This effect is modeled in Eq. (4) by the function c_i which is the ratio of the quantity of dissolved anhydrous to the water content.

$$\begin{cases} c_i = \dfrac{An_{\mathrm{p}_{diss}}}{W_\mathrm{p}} \\ An_{\mathrm{p}_{diss}} = \dfrac{1}{V_{paste_{\mathrm{ini}}}} \left(\dfrac{\alpha_i \cdot m_i}{\rho_i}\right) \end{cases} \tag{11}$$

Where: $-An_{\mathrm{p}_{\mathrm{diss}}}$ is volumetric concentration in paste of dissolved anhydrous phase "i".

We assume that the kinetic activation due to the water supersaturation increases linearly with the degree of hydration, which leads to the above expression for c_i (Eq. (11)). In other words, we assume that the contest between dissolution speed and reactive consumption speed leads to increasing supersaturation.

2.1.4. Secondary pozzolanic reaction delaying parameter

The function "g_i" in Eq. (4) is a factor delaying the hydration kinetics for pozzolanic constituent reactions depending on primary reactions (Eq. (12)).

$$g_i = \begin{cases} C_{p_{CH}} & \text{if } i \neq \text{clinker} \\ 1 & \text{if } i = \text{clinker} \end{cases} \quad (12)$$

Where $C_{p_{CH}}$ is the volumetric concentration of portlandite in the paste.

This means that secondary component reactions cannot occur if the primary reaction is not sufficiently advanced. In the case of fly ash reaction, this kinetic limitation will thus be linked to the portlandite content.

2.2. Water mass balance equation

As for temperature, the water content in concrete is modified by two phenomena: (i) water consumption by hydration or pozzolanic reactions, and (ii) water exchanges with the environment. Its distribution is obtained by resolving the water mass balance equation (Eq. (2)).

The hydric diffusion coefficient governing water transport is strongly dependent on the moisture content of the pore system. Xi [15] reported this nonlinearity and proposed to express this diffusion coefficient D as a function of relative humidity (ψ).

$$D_w(\psi) = D_{w_0}\left[1 + a\left(1 - 2^{-10^{b(\psi-1)}}\right)\right] \quad (13)$$

Where D_{w_0}, a and b are model parameters [16].

In the case of hardening concrete, the moisture transport coefficient also depends on the degree of hydration of the material. Transport is accelerated in the case of fresh concrete, which presents a larger porosity. This effect should be taken into account for precise modeling but, in practice, it would be difficult to take into account the dependence of the diffusion coefficient on the hydration degree because of the diffusion testing protocol, which imposes a long testing time incompatible with a good evaluation of diffusion coefficient modification in hardening concrete.

Therefore in this paper, for the sake of simplification, we neglect the dependence of the moisture coefficient on the hydration degrees. This hypothesis is acceptable if macroscopic hydric transfers in the first few hours remain limited, which occurs during normal curing. Then, the porous structure develops fast enough for Xi's isotherm to be realistic.

Exchanges with the environment may be caused by drying due to convection (Eq. (14)) or by fixed water content (Eq. (15)) (in the case of humid curing for instance).

$$\begin{cases} h_c(W_{air} - W_{face}) \cdot \vec{n} - D_w \cdot \overrightarrow{\text{grad}} W = 0 & (14) \\ W_{face} - W_{imposed} = 0 & (15) \end{cases}$$

Where:

- h_c is the convective exchange coefficient
- W_{air} is the water content in ambient air
- W_{face} is the water content on the external face of the concrete subjected to exchange
- $W_{imposed}$ is the water content imposed on the external face (humid curing for instance)

2.3. Heat balance equation and boundary conditions

The temperature field in the structure is modified by hydration heat production on the one hand and by the boundary conditions (exchanges with environment) on the other. Its distribution is obtained by resolving the heat balance equation (Eq. (3)).

The boundary conditions associated with this equation may be described in three different ways: fixed temperature, exchanges by convection and radiation, and fixed solar flow.

2.3.1. Thermal exchanges by convection

Exchanges by convection and radiation are controlled by simplified equations depending on the temperature gradient between the air and the faces of the structure (Eqs. (16) and (17)).

$$\begin{cases} \varphi_{c+r} \cdot \vec{n} - \lambda \cdot \overrightarrow{\text{grad}} T = 0 & (16) \\ \varphi_{c+r} = H_{eq}(T_{ext} - T_{face}) & (17) \end{cases}$$

Where:

- λ is concrete thermal conductivity
- φ_{c+r} is the global convection and radiation flow
- T_{ext} is the ambient temperature
- T_{face} is the temperature of the face of the concrete block
- H_{eq} is the equivalent heat transfer coefficient defined by Eq. (18)

The equivalent transfer coefficient takes into account convective and radiative exchanges and heat transfer through formwork using classical thermal serial modeling (Eq. (18)).

$$\begin{cases} \dfrac{1}{H_{eq}} = \dfrac{1}{H_{c+r}} + \dfrac{e_f}{\lambda_f} \\ H_{c+r} = H_{rad} + H_{air} \end{cases} \quad (18)$$

Where:

- λ_f is the thermal conductivity of the formwork
- e_f is the formwork thickness
- H_{rad} is the radiative exchange coefficient
- H_{air} is the convective exchange coefficient in air

The convective transfer coefficient H_{air} is determined according to the wind speed (Eq. (19)) [17].

$$H_{air} = a \cdot S_w^b \quad (19)$$

Where:

- a and b are model parameters determined in [17]
- S_w is the wind speed expressed in m/s

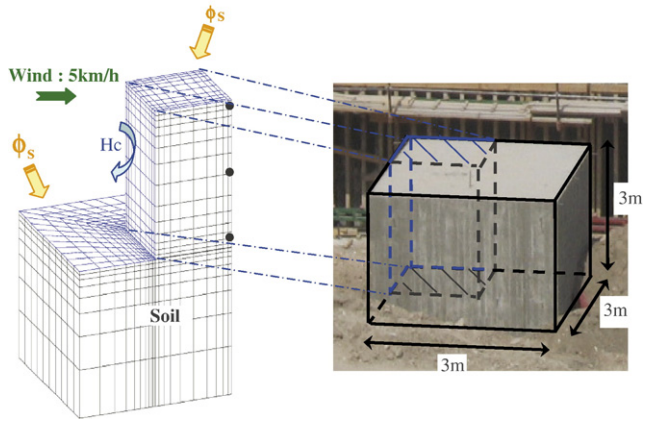

Fig. 1. Concrete test block geometry and associated finite element mesh (only a quarter of the block is simulated to take advantage of the symmetries).

Ambient temperature variations are modeled for instance by a sinusoidal variation fitted on temperature measurements made in situ.

2.3.2. Solar flux evaluation

Solar flux (Eq. (20)) is modeled according to both geographical location and weather. It also takes account of the absorption coefficient of the exposed face $(1-\beta)$.

$$\begin{cases} \varphi_s \cdot \vec{n} - \lambda \cdot \overrightarrow{\text{grad}} T = 0 \\ \varphi_s = (1-\beta) \cdot \varphi_{face} \end{cases} \quad (20)$$

Where:

- $\varphi_{face} = \gamma \cdot \varphi_{max}$ (21)
- β is the face albedo (fraction of solar radiation scattered or reflected)
- γ is a proportionality coefficient modeling the effect of clouds
- φ_{max} is the maximal radiation on the face evaluated from the geographic location, date and hour [18].

2.4. Model calibration method and numerical implementation

As the proposed multiphasic model is based on phenomenological laws, almost all model parameters have a physical meaning and can be calculated from the anhydrous chemical compositions and the concrete formulation, or are drawn from literature. Therefore, the three parameters A, B, and n of the hydration kinetic laws (Eqs. (4) and (5)) must be fitted on experimental results. In this study, they were determined using a quasi adiabatic test performed with a Langavant calorimeter. For calibration, a least squares method was used to determine the material parameters which allow the experimental hydration heat curve to be reproduced.

For the ASTM class F fly ash reaction kinetic law, the thermal activation energy (in function h_i) was calibrated on results obtained by Renedo [19], who performed a test of ASTM class F fly ash hydration in calcium solution for different temperatures (93.75 g of fly ash for a solution of 56.25 g of $Ca(OH)_2$ in 1.5 l of water). His results are representative of the temperature effect on the reaction kinetics of fly ash itself (without interaction with clinker hydration). The three fitting parameters (A, B, n) were then calibrated using results from a Langavant test performed on a binder composed, in this case, of 60% clinker and 40% fly ash.

Table 1
Concrete formulation

Material	Content (kg/m^3)
Cement (CEM I 42.5N)	210
Fly ash	140
Sand 0/4 mm	763
Gravel 4/16mm	567
Gravel 16/32 mm	574
Plasticizer	4
Effective water	131

Table 2
Boundary condition model parameters

Parameter	Value	Determination method
a	7.3	[14]
b	0.78	
S_w (m/s)	2.78	
H_{air} (J/(h·m^2·K))	33,955	(Eq. (19))
H_{rad} (J/(h·m^2·K))	20,276	
λ_f (J/(h·m·K))	540	Drawn from literature for plywood [15]
e_f (m)	0.021	
H_{eq} (J/(h·m^2·K))	17,443	(Eq. (18))
φ_{mean} (J/(h·m^2))	2.73E6	[15]
β	0.2	
γ	0.38	

3. Application to in situ instrumented structure

3.1. Structure modeled

The hydration model presented in Section 2 was applied to an actual massive structure in order to forecast the temperature state variation in concrete. The structure studied was a cubic test block (27 m^3) made to assess, in a realistic environment, the

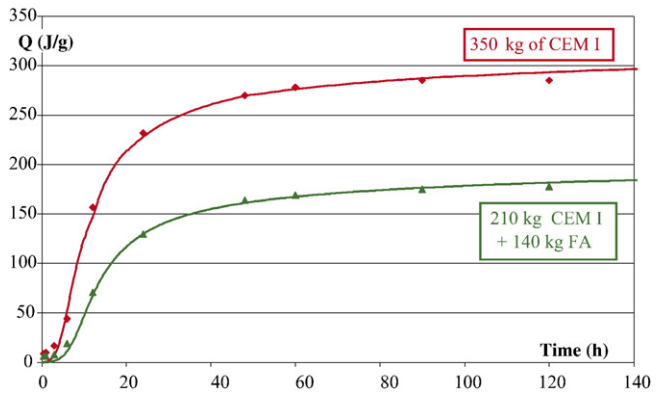

Fig. 2. Calibration of kinetic hydration law on experimental values of heat produced in Langavant calorimetric test.

Table 3
Hydration kinetics model parameters

Component				
Equation	Parameter	Clinker	Fly ash	Determination method
Global kinetic law (Eq. (4))	A_i	1.10E5	1.32E12	Fitting parameter
Water accessibility (Eqs. (5)–(9))	B_i	1.565	7.139	Fitting parameter
	n_i	0.531	0.172	Fitting parameter
	ρ_i (kg/m^3)	3224	2200	Calculated from Bogue formula (clinker) and drawn from [8] (fly ash)
	R_i (m^3/m^3)	1.83	1.94	Calculated from chemical composition (clinker) and drawn from [8] (fly ash)
Thermal activation (Eq. (10))	E_{a_i}/R (K^{-1})	3200	6800 [16]	

Table 4
Thermal characteristics of concrete and soil

Parameter	Value	Determination method
λ_c (J/(h·m·K))	6480	Drawn from literature for this concrete type (mass concrete) [15]
c_c (J/(kg·K))	900	
ρ_c (kg/m^3)	2433	In situ measurement
λ_s (J/(h·m·K))	2340	Drawn from literature for this soil type [15]
ρ_s (kg/m^3)	2000	
c_s (J/(kg·K))	800	
Q^T_{th} clinker (J/g)	437	Calculated from Bogue formula [17]
Q^T_{th} fly ash(J/g)	570	Literature [8]

thermal behavior of the concrete used for the construction of the massive parts of the Naga Hammadi dam over the Nile river (Egypt) by VINCI Construction Grands Projets. Its geometry is represented in Fig. 1.

The general multiphasic hydration model was here applied to 3 phases (2 solid and 1 liquid) (Eq. (22)).The 2 solid phases were clinker (c) and fly ash (fa).

$$\begin{cases} \dot{\alpha}_c = \mathsf{F}(\alpha_c, W, T) \\ \dot{\alpha}_{fa} = \mathsf{F}(\alpha_{fa} W, T) \\ \dot{W} = div(-D_w \cdot \overrightarrow{\text{grad}} W) + Q^W_{th_c} \cdot \dot{\alpha}_c + Q^W_{th_{fa}} \cdot \dot{\alpha}_{fa} \\ \rho c \cdot \dot{T} = div(-\lambda \cdot \overrightarrow{\text{grad}} T) + Q^T_{th_c} \dot{\alpha}_c + Q^T_{th_{fa}} \cdot \dot{\alpha}_{fa} \\ +\text{boundary and initial conditions} \end{cases} \quad (22)$$

Where $Q^W_{th_c}$ and $Q^T_{th_c}$ were calculated from the cement mineral composition [20].

In order to forecast the temperature in the test block, not only the concrete block but also the soil had to be modeled. Indeed, heat transfers by conduction are allowed between the two materials, which can significantly modify the temperature field.

The test block was made using CEM I 42.5N cement based concrete. The concrete formulation is presented in Table 1.

The lateral faces of the concrete block were subjected to thermal exchanges by convection and radiation modeled by the simplified equations previously presented in Eqs. (16)–(18).

The equivalent transfer coefficient H_{eq} and external temperature T_{ext} were determined using Eqs. (18) and (19), the different parameters for which are given in Table 2.

Upper horizontal face of the concrete block was not protected by formwork and was subjected to an equivalent convective coefficient of free face ($H_{c+r}=H_{rad}+H_{air}$).

From the hydric point of view, the structure was isolated from exchanges with the surroundings by formwork on the lateral faces and by application of a curing product to the upper horizontal face.

3.2. Determination of multiphasic model parameters

As previously seen, the hydration law parameters used in Eqs. (4)–(10) were obtained using the results of a Langavant calorimetric test. The variations in heat production deduced from this test are presented in Fig. 2, where the points represent experimental results and the curve the theoretical variation obtained with the fitted parameters of the two species studied (clinker and fly ash) presented in Table 3.

The clinker hydration kinetic law obtained with these calibrated parameters is plotted in Fig. 3. We chose to express this law according to hydration degree in order to compare it with the kinetic expressions used in earlier works. It can be seen that the law shape is similar to those presented by Ulm [21]. We can also refer to Bernard [22], who presents several analytic equations for this law which give a similar shape.

Numerical resolution of the multiphasic model equation (Eq. (22)) requires a determination of the thermal and hydric

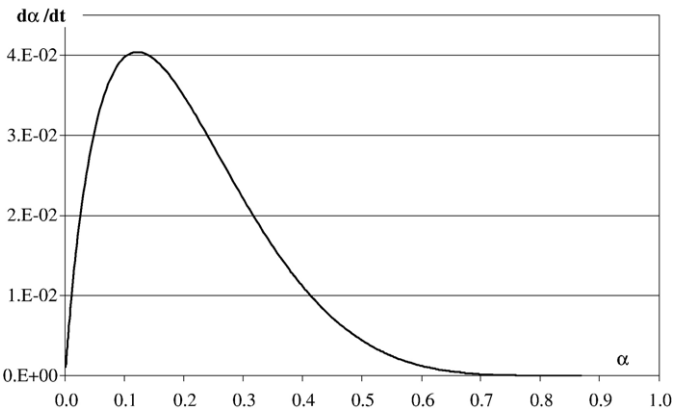

Fig. 3. Variation of clinker hydration kinetics law according to hydration degree.

Table 5
Hydric characteristics of concrete

Equation	Parameter	Value	Determination method
Hydric transfer coefficient (Eq. (13))	D_0	1E−11	[13]
	a	6	
	b	2	
(Eq. (22))	Q^W_{th} clinker (m^3/m^3)	0.32*m$_{clinker}$	[17]
	Q^W_{th} fly ash (m^3/m^3)	0.75*m$_{fa}$	[8]

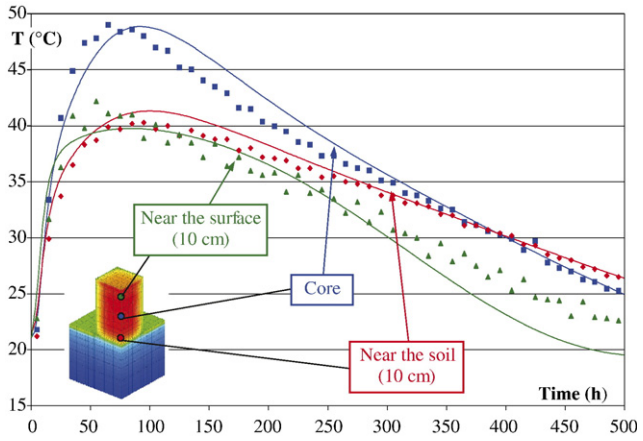

Fig. 4. Temperature variations for different points of concrete block: comparison between experiment (points) and model (curves).

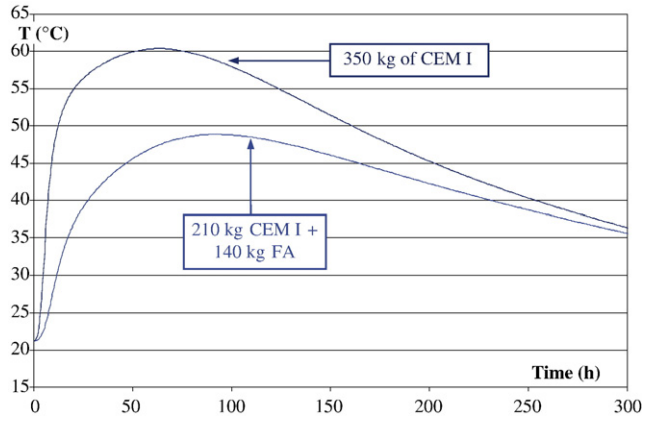

Fig. 6. Concrete block core temperature variation for two types of binders (clinker and blended cement).

characteristics of the material used. These parameters are presented in Tables 4 and 5. In both tables we also present the method used to determine each parameter.

3.3. Model validation on this structure

The calculations on the structure presented in Fig. 1 were performed by implementing the model in the finite element code CASTEM2000 [23].

Fig. 4 illustrates temperature variation versus time. It allows the model results to be compared with experimental ones obtained on the block in situ, for which three measurement locations were considered: in the concrete block core, at 10 cm from the upper surface of the concrete and at 10 cm from the contact surface between soil and concrete.

It can be seen that the temperature variation at each measurement point is quite well reproduced by our model.

3.4. Complementary parametric study

In this part of the work, we used our calibrated multiphasic model to perform a parametric study and to evaluate the influence of cement type and boundary conditions on temperature variation in the concrete block.

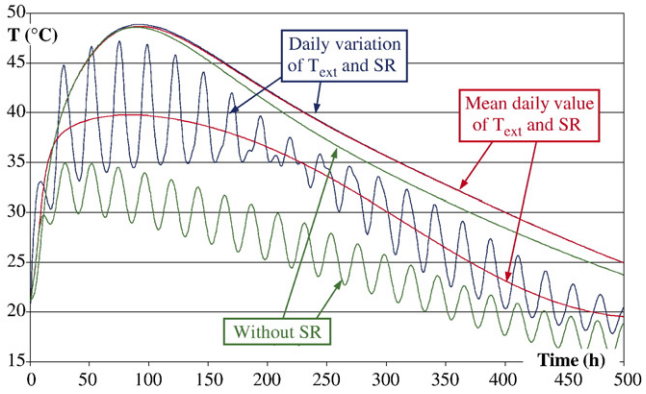

Fig. 5. Temperature variation in concrete block for different ambient conditions (T_{ext}: ambient temperature, SR: solar radiation) (for the color convention see Fig. 4) (For interpretation of the references to color in this figure legend, the reader is referred to the web version of this article.)

3.4.1. Effect of thermal boundary conditions

The effects of temperature daily variation and of solar radiation on the concrete block temperature are illustrated in Fig. 5, where temperature is plotted versus time for two locations in the concrete block (in the core and 10 cm from the upper surface of the concrete), and for different external conditions. The first calculations were performed considering daily variations of both temperature (T_{ext}) and solar radiation (SR). The simulation in which the daily variation of temperature and solar radiation are neglected is also given on the figure for ease of comparison. Finally computations were made with only exchanges with the surroundings due to external temperature (with daily variation); solar radiation was not taken in account.

It can first be noted that the core temperature was not affected by the fact that we neglected daily variations of temperature or solar radiation (core temperature curves are superposed). These simplifications only affected the surface temperature.

Fig. 5 shows that the influence of solar radiation (in this climatic configuration) is higher than that of temperature daily variation. Neglecting the latter only smoothens surface temperature variation but does not affect the mean value. In contrast, the presence of solar radiation also modifies the mean value and neglecting it leads to an underestimation of the surface temperature.

3.4.2. Effect of mineral additions

Fig. 6 points out the influence of the binder nature on the concrete block core temperature.

This figure highlights the influence of binder composition on core temperature variation. As expected, partial replacement of cement by fly ash reduces the maximal temperature. But the simulation also shows slower heat development kinetics due to this substitution. This reduction is explained by a reduction in clinker hydration due to the delaying effect of fly ash. This delaying effect has been experimentally illustrated by Schindler [24].

4. Conclusions

A numerical model predicting the hydration development of multicomponent cement-based materials has been proposed. Based on a multiphasic approach, which is its original feature, the model allows the coupling of several solid phases with environmental conditions. It was built to predict the variation of multicomponent hydration not only in endogenous conditions but also in in situ conditions, where the effects of water exchange (gain or loss), solar radiation and wind are not negligible.

Application to the concrete cube ($3 \times 3 \times 3$ m^3) in situ gave results in good agreement with the experimental ones.

Parametric study results pointed out the efficiency of this multiphasic model in the preliminary design phase, where it can help with the choice of materials and concrete processing (formwork, cure, phasing) according to criteria chosen for temperature variation (T_{max} and/or kinetic) and the correlated risk of early age cracking.The use of the model for predictive simulations performed in a preliminary design phase of massive structure construction is also simplified because model calibration only requires a semi-adiabatic calorimetry test.

Acknowledgments

The authors acknowledge the technical and financial support of the French Group *VINCI Construction Grands Projets* and particularly thank Laurent Boutillon and Lionel Linger from the Scientific Department for their collaboration and expertise.

We are also grateful to *CEA/DEN/DM2S/SEMT* for providing the finite element code CASTEM2000.**[KS]**

References

[1] D.P. Bentz, 'CEMHYD3D: A Three-Dimensional Cement Hydration and Microstructure Development Modelling Package. Version 2.0', NISTIR 6485, U.S. Department of Commerce, April 2000.
[2] K. Meakawa, R. Chaube, T. Kishi, Modeling of concrete performance: hydration, microstructure formation and mass transport, E and FN SPON, London, 1999.
[3] K. van Breugel, Numerical simulation of hydration and microstructural development in hardening cement-based materials, Cem. Concr. Res. 25 (2) (1995) 319–331.
[4] G. De Schutter, Specific heat and thermal diffusivity of hardening concrete, Mag. Concr. Res. 47 (172) (1995) 203–208.
[5] G. De Schutter, Hydration and temperature development of concrete made with blast-furnace slag cement, Cem. Concr. Res. 29 (1999) 143–149.
[6] T. Kishi, K. Maekawa, Thermal and mechanical modelling of young concrete based on hydration process of multi-component cement materials, Thermal cracking in concrete at early age, RILEM Proc. 25 (1994) 11–19.
[7] T.C. Powers, T.L. Brownyard, Studies of the physical properties of hardened Portland cement paste, Part 9, ACI J. 18 (8) (1947).
[8] T.C. Hansen, Physical structure of hardened cement paste, a classical approach, Mat. Struct. 19 (114) (1986) 423–436.
[9] D.P. Bentz, Influence of water-to-cement ratio on hydration kinetics: simple models based on spatial considerations, Cem. Concr. Res. 36 (2006) 238–244.
[10] B.H. Oh, S.W. Cha, Nonlinear analysis of temperature and moisture distributions in early-age concrete structures based on degree of hydration, ACI Mater. J. 100 (5) (2003) 361–370.
[11] V. Waller, Relations composition des bétons, exothermie en cours de prise et résistance en compression, Thèse de Doctorat (1999), ENPC Paris, 297 p.
[12] G. Parry-Jones, A.J. Al-Tayyib, A.I. Mana, Evaluation of degree of hydration in concrete using ^{29}Si magic angle spinning NMR in solids, Cem. Concr. Res. 18 (2) (1988) 229–234.
[13] S. Arrhenius, Quantitative Laws in Biological Chemistry, G. Bell and Sons, London, 1915.
[14] H.F.W. Taylor, Cement Chemistry, Academic Press, New York, 1990.
[15] Y. Xi, Z.P. Bazant, L. Molina, H.M. Jennings, Moisture diffusion in cementitious materials: moisture capacity and diffusivity, Adv. Cem. Based Mater. 1 (1994) 258–266.
[16] S. Poyet, Etude de la dégradation des ouvrages en béton atteints par la réaction alcali-silice: approche expérimentale et modélisation numérique multi-échelles des dégradations dans un environnement hydro-chemo-mécanique variable, Thèse de Doctorat (2003), Université de Marne La Vallée, 238 p.
[17] W.H. McAdams, Heat Transmission, McGraw Hill Series in Chemical Engineering, McGraw Book Company, New York, 1954.
[18] C.A. Roulet, Energétique du bâtiment I: intéractions entre le climat et le bâtiment, Presses Polytechniques Romandes, Lausanne, 1987 (in French).
[19] M.J. Renedo, J. Fernandez, Kinetic modelling of the hydrothermal reaction of fly ash, $Ca(OH)_2$ and $CaSO_4$ in the preparation of desulfurant sorbents, Fuel 83 (2004) 525–532.
[20] A.M. Neville, Properties of Concrete, 4th edLongman, 1995.
[21] F.-J. Ulm, O. Coussy, Couplings in early-age concrete: from material modeling to structural design, Int. J. Solids Struct. 35 (31–32) (1998) 4295–4311.
[22] O. Bernard, F.J. Ulm, E. Lemarchand, A multiscale micromechanics-hydration model for the early age elastic properties of cement-based materials, Cem. Concr. Res. 33 (2003) 1293–1309.
[23] Commissariat à l'Energie Atomique CEA — DEN/DM2S/SEMT, CASTEM2000, web page: http://www-cast3m.cea.fr/cast3m/index.jsp.
[24] A.K. Schindler, K.J. Folliard, Influence of supplementary cementing materials on the heat of hydration of concrete, Advances in Cement and Concrete IX Conference, Copper Mountain Conference Resort in Colorado, August 2003, 10 pp.